

iAssistADL: Intelligent assistive device for patients with neurodegenerative movement disorder: Concepts and first implementations

Winfried Ilg¹, Isabell Wochner², Jhon P.F. Charaja¹, Veronika Hofmann^{4,5}, Ole Streng^{4,5}, Melanie Adam¹, Regine Lendway¹, Jan Kerner¹, Bhavya Deep Vashisht², Marko Ackermann^{2,9}, Friedemann Bunjes¹, Urs Schneider^{4,5}, Martin Giese¹, Andreas Bulling⁶, Syn Schmitt⁷, Christophe Maufroy^{4,5} and Daniel Haeufle¹

Abstract—Upper-limb activities of daily living like eating and drinking are crucial for self-determination and autonomy and, thus, quality of life. Patients with neurodegenerative diseases such as Parkinson’s disease, multiple sclerosis or cerebellar ataxia are often severely impaired in performing these activities of daily living. While these patients are still able to plan motor actions, and their muscle strength is rarely impaired, tremor or overshooting movements disturb the intended movements. This occurs progressively in the course of disease in a way that independent eating and drinking becomes increasingly difficult. The goal of this research project is to develop a non-invasive assistive device suppressing pathological movement components while allowing intended movement. The newly designed hardware will be controlled by a combination of computational methods to detect user intention, detect pathological movement components within intended movements, and predict the required correction forces for several upper-limb activities of daily living. In this manuscript, we will describe concepts of control hard- and software as well as first implementation and experiments with the individual components we plan to integrate in the future.

I. INTRODUCTION

Cutting food or filling a glass from a bottle while dining is crucial for self-determination and autonomy and, thus, quality of life. Patients suffering from neurodegenerative diseases, such as Parkinson’s disease, multiple sclerosis or cerebellar ataxia might not be able to perform such activities of daily living (ADL) all the time.

Although these patients are able to plan motor actions, and their muscle strength is rarely impaired, different types of tremor [1] [2] or dysmetric movements (over- and under-shooting of goal-directed movements in cerebellar ataxia) [3] [4] [5] disturb the intended movements.

This occurs progressively in the course of disease such that independent eating and drinking becomes increasingly difficult. Assistive devices, which pro-actively suppress patholog-

ical movement components and restore the intended movement could dramatically improve patients’ motor abilities, as has been shown in approaches to wearable systems for tremor suppression [6].

We here address the field of ADL with the focus on situations like a regular meal where food has to be cut, forked, brought to the mouth and a glass of water has to be filled from a bottle and brought to the mouth. These activities are characterized by a finite number of objects and tasks, a meaningful order of some tasks, but generally open in the location of objects and user and situation-specific in their execution order.

The goal of this research project is to develop a non-invasive assistive device with the capability to suppress pathological movement components while allowing intended movement in patient-relevant ADLs.

A. Methodological Approach

We address the following challenges in the development of such assistive devices:

- 1) Predicting planned movements during ADL and detecting pathological movement components within executed movements in real-time.
- 2) Designing a lightweight and mobile assistive device with minimal mechanical complexity and sufficient transparency (to not hinder the movement of the user) and, at the same time, the capacity to apply in real-time the amount of corrective forces sufficient to suppress pathological movement components.

To this end, we combine computational methods to detect (a) the user intention, predict the human arm movement corresponding to the intention, (b) differentiate between desired movement and pathological movement components and (c) develop a neuromechanical model to predict the required correction forces and (d) apply them with an adequately designed assistive device (Figure 1).

The presented concepts differ significantly from concepts for stroke patients, where paralysis of the limbs or spasticity is the main issue (e.g. [7],[8]). Devices for stroke need to exert forces large enough to generate the entire movement and—typically slowly—follow given trajectories, thus, they typically place fewer demands on the real-time constraints in intention detection [9] and movement correction [6].

This paper reports about the overall concept and our first implementations and test of the sub-components. At this

*corresponding author: daniel.haeufle@uni-tuebingen.de, ¹Hertie Institute for Clinical Brain Research, and Centre for Integrative Neuroscience, University of Tübingen, Germany. ²Institute of Computer Engineering (ZITI), Heidelberg University, Germany. ³Max Planck Institute for Intelligent Systems, Tübingen, Germany. ⁴Institut für Industrial Manufacturing and Management (IFF), University of Stuttgart, Germany. ⁵Fraunhofer Institute for Manufacturing Engineering and Automation (IPA), Stuttgart, Germany. ⁶Institute for Visualization and Interactive Systems, University of Stuttgart, Germany. ⁷Institute for Modelling and Simulation of Biomechanical Systems, University of Stuttgart, Germany. ⁸Department of Computer Science, University of Tübingen, Germany. ⁹Institute for Anthropomatics and Robotics, Karlsruhe Institute of Technology, Germany.

This work was financed by the Baden-Württemberg Stiftung in the scope of the AUTONOMOUS ROBOTICS project *iAssistADL* granted to WI, MG, SS, and DH.

point, these components are not integrated yet leaving the validation of the concept as future work.

II. METHODS

A. Multi-modal sensor setup

Multiple sensor modalities were captured synchronously to assess the subject’s motion behaviour and infer the intention (Figure 2). To determine gaze direction in real-life scenarios, we used the eye tracking glasses Neon by PupilLabs (Pupil Labs GmbH, Berlin, Germany) [10], which additionally record a video from the egocentric perspective and give information about head movements via an inertial sensor. Multiple IMUs from Xsens Technologies (Movella DOT, Xsens Technologies B.V., Enschede, Netherlands) were placed on both arms and the sternum to track and quantify arm and trunk movements. The stereo depth camera ZED 2i from Stereolabs (Stereolabs Inc., San Francisco, USA) were placed across the table of the subjects and captures the depth and RGB information of the experimental setup. Based on this depth and RGB information, object recognition and skeleton tracking routines were implemented using the camera-related APIs. Fusion of the IMU and depth-camera sensor signals allows for combining the benefits of both sensors: high time-resolution and local accuracy of IMU’s and global position accuracy of the depth-image to compensate for drift in the IMU signals. Details of the sensor fusion concept are provided in the next section.

A software architecture based on the ROS2 (Robot Operating System) middleware was implemented to acquire all sensors synchronously with the sensor-specific real-time constraints. ROS2 provides the ability to reliably exchange and store large amounts of data at high frequency and is widely used in medical and industrial applications [11] [12] [13].

B. Development of a Kalman filter-based sensor fusion algorithm for motion tracking

Intention detection, tremor recognition, and prediction of movements require sensor-fusion approaches to combine different sensor modalities. To perform robust motion tracking, we developed and evaluated a Kalman filter-based algorithm for motion tracking and state estimation. The primary aim was to integrate data from multiple sensors to achieve accurate tracking of upper limb motion, particularly the hand and wrist. For this, we combined the complementary strengths of two sensors: the Xsens Movella DOT IMU system, which provides fast precise acceleration and angular velocity data but shows a drift when estimating global positions, and the Stereolabs ZED 2i stereo camera with skeleton fitting, which delivers global 3D position data, but at a lower frequency.

The Kalman filter was selected for its ability to perform real-time state estimation in dynamic systems. Specifically, we employed a discrete-time linear Kalman filter to estimate the states of position, velocity, and acceleration. The filter’s structure consists of a prediction step, which uses a kinematic motion model to estimate the next state based on the current state, and an update step, which refines this estimate using

sensor measurements. In the filter, weights were assigned to each sensor based on their noise characteristics, ensuring robust performance even under noisy conditions.

The state transition model for the Kalman filter estimates the position \mathbf{x} , velocity \mathbf{v} , and acceleration \mathbf{a} of the wrist. The discrete state-space model can be expressed as:

$$\mathbf{s}_{k+1} = \mathbf{F}\mathbf{s}_k + \mathbf{w}_k, \quad \mathbf{z}_k = \mathbf{H}\mathbf{s}_k + \mathbf{v}_k$$

where

$$\mathbf{s}_k = \begin{bmatrix} \mathbf{x}_k \\ \mathbf{v}_k \\ \mathbf{a}_k \end{bmatrix}, \quad \mathbf{F} = \begin{bmatrix} \mathbf{I} & \Delta t \mathbf{I} & \frac{\Delta t^2}{2} \mathbf{I} \\ \mathbf{0} & \mathbf{I} & \Delta t \mathbf{I} \\ \mathbf{0} & \mathbf{0} & \mathbf{I} \end{bmatrix}, \quad \mathbf{H} = \begin{bmatrix} \mathbf{I} & \mathbf{0} & \mathbf{0} \\ \mathbf{0} & \mathbf{0} & \mathbf{I} \end{bmatrix},$$

where \mathbf{F} is the state transition matrix, \mathbf{H} is the measurement matrix, \mathbf{w}_k and \mathbf{v}_k are the process and measurement noise, respectively, and Δt is the sampling time.

To evaluate the filter’s performance, we first designed a testing framework using an ideal trajectory overlaid with experimentally derived noise. Noise profiles for the IMU and stereo camera were characterized through calibration experiments, where the sensors were subjected to static placement evaluation to get their base noise readings. The accelerometer’s and stereo camera signal variances were used to estimate the measurement noise covariance matrix.

The primary metric for evaluating performance was the Root Mean Square Error (RMSE) of the reconstructed trajectory compared to the ground truth. Ground truth data was generated using (a) mathematical simulation and (b) a high-accuracy optical motion capture system, which provided precise positional and velocity measurements for the ideal trajectory. By calculating the RMSE, we assessed the algorithm’s accuracy in estimating states under various noise levels.

Finally, the sensor fusion approach was validated using real experimental data. This included datasets captured with both the IMU and stereo camera in scenarios simulating upper-limb motion. The fusion algorithm was tested in realistic conditions, accounting for sensor noise, data loss, and calibration challenges.

C. Online detection of pathological movement components

For the detection of pathological movement components, we concentrated on tremors and dysmetric movements (over- and undershooting). In the case of tremors, we have to take into account that the frequency of the tremor may change within the movement in the action and intention tremors. Therefore, we used a Bandlimited Multiple Fourier Linear Combiner improved with a Kalman Filter [14] to estimate the sinusoidal movements with changing frequencies to identify the tremor component of the voluntary motion in real-time. See subsection III-B for preliminary results.

D. Neuromechanical modeling of healthy and impaired movement

Using neuromusculoskeletal arm simulations, we can predict both healthy and impaired movements and estimate the necessary assistive forces for correction [15]. These

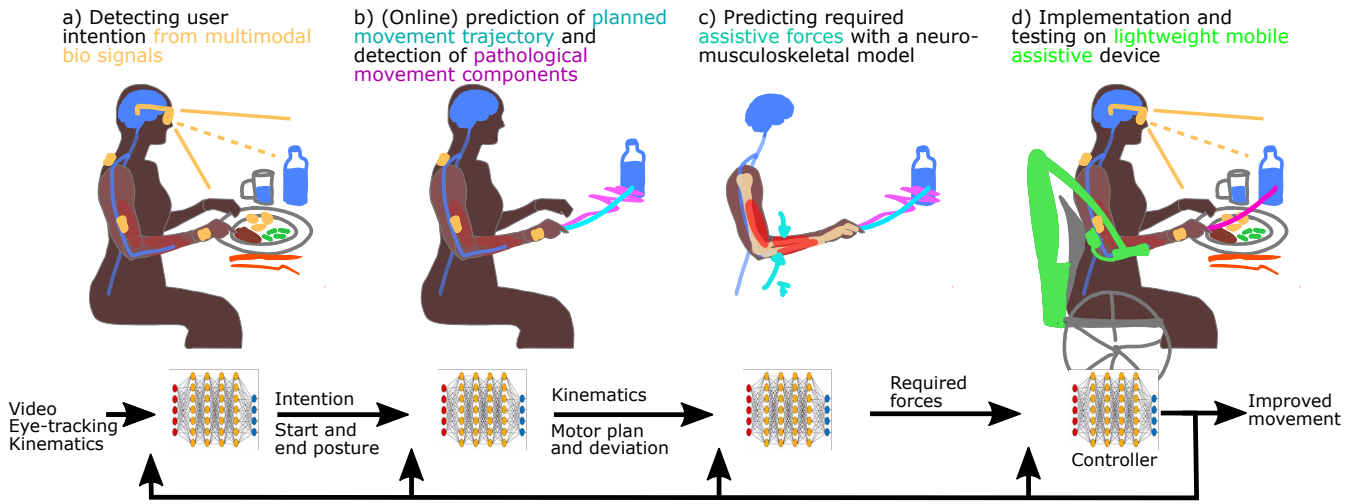


Fig. 1: Overview of the overall control architecture and its individual components.



Fig. 2: The used sensor modalities to collect various data. a) ZED2i stereo camera b) Movella DOT IMUs c) Eye tracking system Pupil Labs Neon.

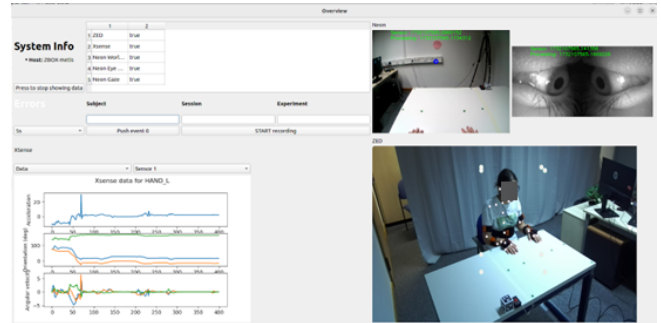


Fig. 3: Screenshot of the Graphical User Interface. System information is shown on the top left, including possible runtime errors such as data loss due to restricted data buffer size. It also features the recording control and a button for event generation. Live data of the motion sensor is shown below. The two top right shows the eye-tracking system with an overlay of gaze data and timestamps. Bottom right shows the RGB image of the ZED2i, overlaid with skeleton data.

predictions help to determine the corrective forces required as control inputs to the assistive device, which, in turn, will in the future apply forces to the human arm to correct dysfunctional movements (see Figure 1 c)).

To predict healthy movements, we developed a simulation approach for 3D arm movements that integrates three key factors: optimality principles, task requirements, and stochastic noise. Muscle and multibody dynamics were simulated using the MuJoCo physics engine [16] due to its computational speed and applied reinforcement learning (DEP-MPO) [17] to synthesize the control policy. We build on our previous work with a simplified, two degree-of-freedom arm model with six muscles-tendon units [18]. In this work, we achieved highly realistic arm trajectories (realism index > 0.9), comparable to those of healthy individuals.

Expanding this framework, we tested a more complex model with seven degrees of freedom and 27 muscle-tendon units (see Fig. 4). Our prior work showed that this 3D arm model predicts stiffness characteristics that closely match experimental data recorded from data while still being computationally efficient [19]. This model therefore allows us to predict the effect of corrective forces for our assistive device

when attempting to mitigate the effects of motor control impairments.

As a first attempt to simulate pathological movement components, we added a sinusoidal signal to the elbow flexor muscle with frequencies occurring in the targeted diseases and varying amplitudes, generating stereotypic tremor movements (Fig. 4). Albeit its simplicity, this isolated approach is beneficial to determine (joint-)specific correction forces. However, we aim at simulating more naturalistic tremors in the future, by transferring our own and previous experimental data onto the model [20], [15] and by considering neurological origins of dysmetria and tremor [21], [22], [23].

E. Design requirements and hardware development

A lightweight assistive device, schematically represented in Fig. 5, was devised to apply corrective forces. It includes a prismatic joint along the z-axis, enabling force application in the vertical direction (blue), along with two revolute joints arranged in series (both axes parallel to the z-axis) in red and green, which mimic the human shoulder and elbow joints. This coordinated arrangement allows for the application of forces in any direction within the horizontal

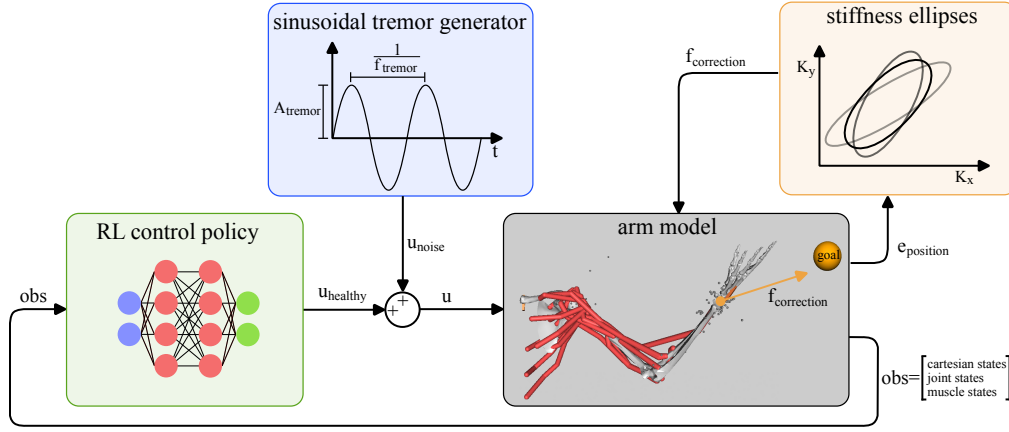


Fig. 4: Simulation of pathological arm movement: RL control policy computes the muscle control command (u_{healthy}) to generate healthy arm movements, while a sinusoidal tremor generator produces a perturbation signal (u_{noise}) with characteristic amplitude ($a_{\text{tremor}} = 0.25$) and frequency ($f_{\text{tremor}} = 4 \text{ Hz}$). This perturbation is added to the muscle control command to simulate hand tremors. Finally, corrective forces ($f_{\text{correction}}$) are computed based on stiffness ellipses and position deviation to attenuate hand oscillations.

plane. Although preliminary investigations in simulation suggested that a force of 5 N applied to the hand can already effectively reduce or prevent the aforementioned movement disorders, the device was designed to provide a force of 10 N to account for the more proximal point of application of the corrective forces (forearm) and potential intersubject variability. We chose a bi-articular actuation scheme for the elbow joint actuation, spanning both the shoulder and elbow joints, as simulations indicated that this approach reduces the maximum torque required by the shoulder actuator compared to a mono-articular elbow actuation scheme. Two mechanisms were used to relocate both shoulder and elbow actuators proximally with respect to the vertical prismatic joint: a ball spline mechanism was utilized to transmit the shoulder actuator moment through the linear bearing of the prismatic joint, while a cable transmission was integrated into the scissor mechanism that connects the prismatic joint output to its driving actuator. The integration of the scissor mechanism also facilitated the compact incorporation of a spring mechanism for passive weight balancing of the robotic arm (see Fig. 5(a)(1)). As all three actuators were attached to the base of the device, the moving part of the designed robotic arm is lightweight and exhibits low apparent inertia, which positively contributes to reducing resistance to user movement when no correction is needed.

A mechanical interface (see Fig. 5 (b)) fixed at the tip of the robotic arm facilitates the application of corrective forces to a point approximately located at the midpoint of the user’s forearm, thus enabling the generation of corrective moments at both the elbow and shoulder. This interface employs a mechanism similar to a gimbal, ensuring that the applied force is centered relative to the forearm, thereby preventing the generation of parasitic moments. The interface was constructed with two passive revolute joints, with the freedom of rotation along the forearm’s longitudinal axis provided by the relative motion of soft tissues with respect to the user’s skeleton. The mechanical interface also extends to the wrist, allowing for the application of forces along the longitudinal axis of the forearm with minimal slippage.

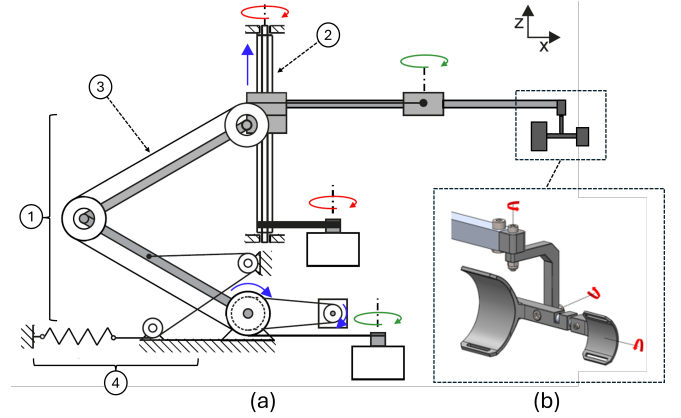


Fig. 5: (a) Schematic of the assistive device with three active DoF. From proximal to distal: a prismatic joint along the z-axis (blue) actuated via a scissor mechanism (1) which motion is constrained by the ball spline mechanism (2), a first rotational joint along the ball spline axis (red) and a second rotational joint bilaterally actuated using cables (3) routed through the scissor mechanism (green). All actuators are fixed to the base of the device, which significantly lowers the mass of the mobile part (arm) of the device. A passive spring mechanism (4) is used to balance the weight of the arm. (b) Close-up of the user interface with 3 passive DoF.

A preliminary evaluation study was performed with the unactuated device. First, we measured the resistive torques or forces experienced when moving each robotic arm DoF with joint velocities typical for the envisioned ADL. Second, we carried out a study with 5 healthy individuals to evaluate the device transparency (Task 1) and range of motion (Task 2). In Task 1, the subjects performed the ADL “Drinking” (fill a glass with the bottle using their right hand and then drink the water from the glass) with the device and were asked to rate from 0 to 10 how much the device was disturbing them (<3: not disturbing; 4-6: little disturbing; >7: very disturbing). In Task 2 the participants were instructed to sequentially place the bottle as close as possible to the four corners of a rectangular workspace drawn on the table in front of them, while avoiding to lean forward.

F. Experimental data acquisition

To achieve the project goal, a novel dataset will be recorded that includes kinematic data, gaze data, and scene

video including depth information (approved by the local ethics committee in Tübingen 474/2023B02). The developed ROS2 software architecture will be used to record a patient group (n = 20) and a group of age-matched healthy controls (n=20).

TABLE I: Planned experimental tasks.

Complex ADLs	Clinical test
Holding an object Peeling, cutting and eating a banana Drinking from a glass Meal preparation	Pointing on the table Moving objects Drawing the Archimedian spiral

The patient group comprises subjects suffering from neurodegenerative diseases such as Parkinson’s disease, multiple sclerosis, or cerebellar ataxia exhibiting ataxic dysmetric movements (over- and undershooting of goal-directed movements in cerebellar ataxia) or tremors such as action and intention tremors.

The participants will be recorded performing different tasks that involve the upper extremities, e.g., meal preparation, while sitting at a table. A standardized data acquisition and experimental protocol was developed. The choice of tasks matches the future application scenario of the assistive device, but also fundamental knowledge is gained about the pathological movements (see Table I). This includes tasks with a high level of standardization and tasks with a higher amount of flexibility.

In the eating task, participants will be instructed to peel a banana, to cut the banana with a knife into smaller pieces, and to eat the pieces with a fork. The drinking task includes opening a bottle and pouring water into a glass. In the context of meal preparation, a Tupperware container is to be opened and the noodles inside emptied into a bowl. The Tupperware box should then be closed. In a follow-up task the noodles should be scooped out from the bowl into a cup using a ladle. The ”clinical test” includes pointing movements at different locations on the table with the index finger, moving wooden bricks from one place to another predefined location, and drawing the Archimedian spiral in the clockwise and anti-clockwise direction.

The experimental protocol will also include a questionnaire to obtain further information that is relevant for analyzing the recorded data and developing the assistive device. The questionnaire covers socio-demographic and anthropometric data on each subject; pathology and associated symptoms; and expectations, doubts and requirements of such a non-invasive assistive device.

III. PRELIMINARY RESULTS

A. Preliminary Results of Kalman Filter

After preliminary data collection, raw data from the IMU and stereoscopic camera were synchronized and pre-processed before being put into the Kalman filter. Preprocessing included removal of gravity component from raw acceleration data, shifting of coordinate systems of the Xsens IMU and the ZED 2i camera, and upscaling data of the stereo camera to match IMU sampling frequency to enable sensor fusion. The coordinate systems of the stereo camera and the

IMU at the wrist were aligned by first translating the origins to the same point and applying a rotation matrix computed using the the Kabsch algorithm [24]. The stereo camera data, although accurate, occasionally suffered from tracking loss, particularly during rapid movements. These limitations were mitigated through the sensor fusion.

In the testing framework using an ideal trajectory as ground truth, the filter achieved low RMSE values of 7.8, 7.8 and 7.4 m^{-4} , in the X , Y , Z directions, respectively. The tests with realistic experimental data demonstrated that the Kalman filter effectively fuses data from the IMU and stereo camera, producing smooth wrist trajectories under varying conditions. The filter successfully estimates motion trajectories while filtering out high-frequency noise.

B. Online detection of pathological movement components

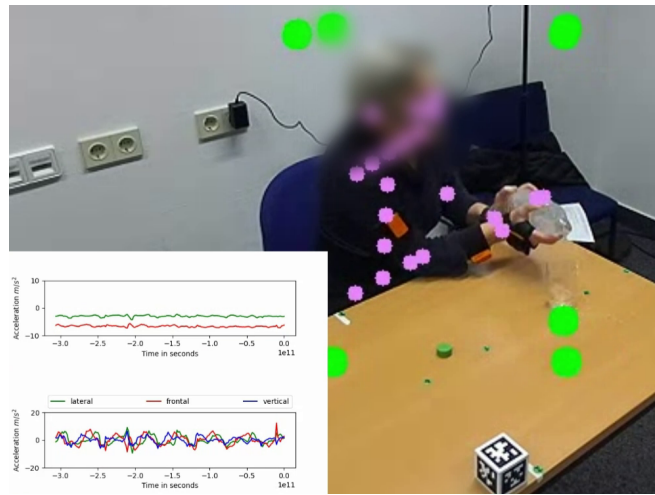


Fig. 6: Snapshot of the recording of the drinking scenario for a tremor patient. Green dots represent the subject’s workspace as identified by the stereo camera. Purple dots show the key points of the skeleton tracking. The left part of the image shows the online tracking of the inertial sensors, showing specific accelerations on the wrist sensor for different subphases of movement.

Results on the data collected so far show varying tremor frequencies not only for different patients but also for the same patient in different phases of movement (Fig. 6 + 7). This reflects the clinical impression of action and intention tremors. Such changing frequencies could be tracked with Bandlimited Multiple Fourier Linear Combiner, improved with a Kalman Filter, to estimate the changing frequencies. It allowed to separate the tremor offline (Fig. 7) and in real-time (Fig. 6). Further approaches will aim to incorporate prior knowledge about patient-specific tremor frequencies in order to optimize fast online detection.

C. Simulation of healthy and impaired arm movement

The synthesized control policy can generate both healthy and impaired point-to-point 3D reaching movements (Fig. 8). On the one hand, the direct application of the muscle control command u_{healthy} resulted in arm reaching movements with healthy kinematics characteristics: (i) roughly straight hand trajectories and (ii) bell-shaped velocity profiles (see early

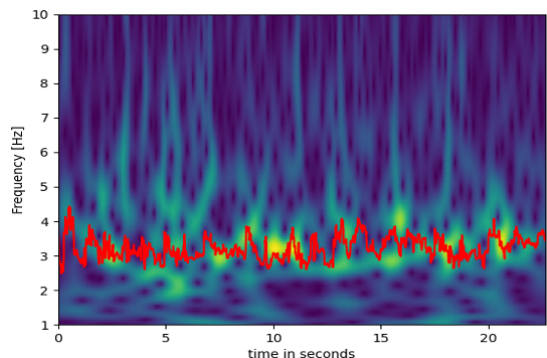


Fig. 7: The bandlimited multiple-fourier linear combiner with Kalman filter adapts to the frequencies of the pathological movement component (red).

reaching phase in Fig. 8, both in healthy and pathological movement). The addition of a sinusoidal signal to the muscle control command of the elbow flexor resulted in periodic positional oscillations around the target position, which is an approximation of tremors.

D. Hardware: Preliminary evaluation of device prototype

The evaluation study (see Fig. 9) revealed that the workspace reachable by the test subjects and available for executing the ADLs was only very marginally (2,2% in average) reduced by the device usage. The test subjects also evaluated positively the mechanical transparency of the device (average rating of 2,2: not disturbing), especially for motions in the horizontal plane but reported a noticeable resistance to vertical motions. This subjective evaluation was confirmed by the quantitative tests: low resistive torques (mean value ≤ 0.1 Nm) were measured for the rotational joints, while a mean resistive force of about 3 N (primarily dry friction) was measured for motions along the z-axis, attributed to internal friction in the ball spline mechanism. In summary, the selected transmission mechanisms, characterized by low internal friction, were shown to enable efficient torque transmission. This design allows using reasonably lightweight motors (approximately 1 kg per actuator) in a quasi-direct drive mode (reduction ratio < 3) to generate the necessary corrective forces. Based on the performance of the direct drive actuation, it is anticipated that interaction forces can be accurately estimated using motor current

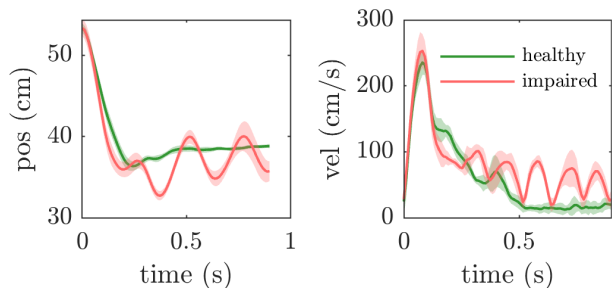


Fig. 8: Neuromechanical simulation of healthy (green) and impaired (red) arm movements. The impaired movement was simulated by adding a sinusoidal signals with frequencies occurring in the related diseases and different amplitudes added to the simulated muscle control signal. Here we show exemplarily 4 Hz and an amplitude of 0.5 (50% maximum muscle stimulation)

measurements in the horizontal plane, whereas active force control may be necessary to compensate for friction in the vertical direction. To address this, a single uniaxial force sensor will be integrated in the next iteration between the arm's tip and the mechanical interface with the user.

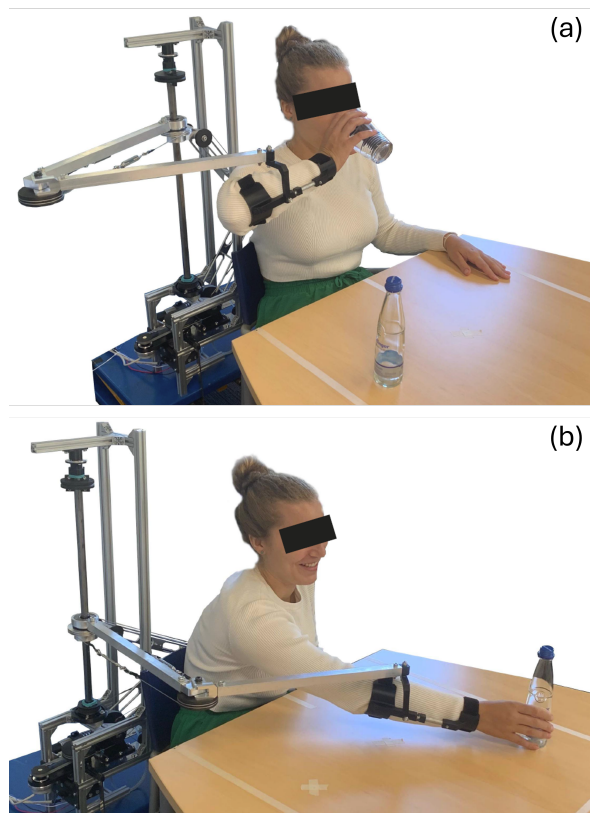


Fig. 9: (a) Subject performing ADL "Drinking", (b) ROM tests.

IV. DISCUSSION

In this manuscript, we presented the concepts and first implementations of the individual components of our hardware and software architecture for an assistive device for patients with neurodegenerative movement disorders like cerebellar ataxia, multiple sclerosis or Parkinson's disease. These specific movement impairments result in pathological movement components overlaying the intended movements. This leads to specific requirements in the hardware and software concepts [15],[6] which differ significantly from concepts for stroke patients, where paralysis of the limbs or spasticity is the main issue (e.g. [7],[8]). Devices for stroke need to exert forces large enough to generate the entire movement and—typically slowly—follow given trajectories or predefined tasks and, thus, they typically place fewer demands on the real-time constraints in intention detection [9] and movement correction [6]. Thus, the two specific aspects of (a) rapid correction of complex everyday movements with (b) a lightweight and low-cost assistive device are the focus of our developments. With the developments and results so far, we have already been able to take some substantial steps in this direction. However, we still develop the individual components. Next steps will include ML methods for intention detection by combining the gaze estimation

of the eye-tracker with the current state of the movement tracking [25]; more naturalistic modeling of dysfunctional movements [23], [22], [15]; prediction of corrective forces with the neuromechanical model [22], [23], [15]; the real-time integration of all components; first user test.

REFERENCES

- [1] M. Sun, W. Jung, K. Koltermann, G. Zhou, A. Watson, G. Blackwell, N. Helm, L. Cloud, and I. Pretzer-Abhoff, "Parkinson's disease action tremor detection with supervised-learning models," in *Proceedings of the 8th ACM/IEEE International Conference on Connected Health: Applications, Systems and Engineering Technologies*, 2023, pp. 1–10.
- [2] D. Paredes-Acuna, N. and Utpadel-Fischler and K. e. a. Ding, "Upper limb intention tremor assessment: opportunities and challenges in wearable technology," *J NeuroEngineering Rehabil*, vol. 21, no. 8, 05 2024.
- [3] N. H. Bhanpuri, A. M. Okamura, and A. J. Bastian, "Predicting and correcting ataxia using a model of cerebellar function," *Brain*, vol. 137, no. 7, pp. 1931–1944, 05 2014.
- [4] K. Oh, D. Cao, N. Cowan, and A. J. Bastian, "Sensitivity of cerebellar reaching ataxia to kinematic and dynamic demands," *bioRxiv*, pp. 2024–10, 2024. [Online]. Available: <https://doi.org/10.1101/2024.10.28.620711>
- [5] D. Hermle, R. Schubert, P. Barallon, W. Ilg, R. Schüle, R. Reilmann, M. Synofzik, and A. Traschütz, "Multifeature quantitative motor assessment of upper limb ataxia including drawing and reaching," *Annals of Clinical and Translational Neurology*, vol. 11, no. 5, pp. 1097–1109, 2024.
- [6] J. S. Lora-Millan, G. Delgado-Oleas, J. Benito-León, and E. Rocon, "A review on wearable technologies for tremor suppression," *Frontiers in Neurology*, vol. 12, 2021.
- [7] R. Hennig, J. Gantenbein, J. Dittli, H. Chen, S. P. Lacour, O. Lambercy, and R. Gassert, "Development and evaluation of a sensor glove to detect grasp intention for a wearable robotic hand exoskeleton," in *2020 8th IEEE RAS/EMBS International Conference for Biomedical Robotics and Biomechanics (BioRob)*. IEEE, 2020, pp. 19–24.
- [8] M. Gardner, C. S. Mancero Castillo, S. Wilson, D. Farina, E. Burdet, B. C. Khoo, S. F. Atashzar, and R. Vaidyanathan, "A multimodal intention detection sensor suite for shared autonomy of upper-limb robotic prostheses," *Sensors*, vol. 20, no. 21, p. 6097, 2020.
- [9] J. Gantenbein, J. Dittli, J. Meyer, R. Gassert, and O. Lambercy, "Intention detection strategies for robotic upper-limb orthoses: A scoping review considering usability, daily life application, and user evaluation," *Frontiers in Neurobotics*, vol. 16, 2022.
- [10] C. Baumann and K. Dierkes, "Neon accuracy test report," 2023. [Online]. Available: <https://zenodo.org/doi/10.5281/zenodo.10420388>
- [11] M. Hutter, C. Gehring, D. Jud, A. Lauber, C. D. Bellicoso, V. Tsounis, J. Hwangbo, K. Bodie, P. Fankhauser, M. Bloesch, R. Diethelm, S. Bachmann, A. Melzer, and M. Hoepflinger, "Anymal - a highly mobile and dynamic quadrupedal robot," in *2016 IEEE/RSJ International Conference on Intelligent Robots and Systems (IROS)*, 2016, pp. 38–44.
- [12] W. Chambers, A. Oyake, M. Deans, K. Hambuchen, and B. Roberts, "Space robot operating system (space ros)," in *ROS Conference (ROSCon) 2021*, 2021.
- [13] H. Saeidi, J. D. Opfermann, M. Kam, S. Raghunathan, S. Leonard, and A. Krieger, "A confidence-based shared control strategy for the smart tissue autonomous robot (star)," in *2018 IEEE/RSJ International Conference on Intelligent Robots and Systems (IROS)*, 2018, pp. 1268–1275.
- [14] K. C. Veluvolu and W. T. Ang, "Estimation of physiological tremor from accelerometers for real-time applications," *Sensors*, vol. 11, no. 3, pp. 3020–3036, 2011.
- [15] Z. Habibollahi, Y. Zhou, M. E. Jenkins, S. J. Garland, M. D. Naish, and A. L. Trejos, "Multimodal tremor suppression of the wrist using fes and electric motors—a simulation study," *IEEE Robotics and Automation Letters*, vol. 8, no. 11, pp. 7543–7550, Nov. 2023.
- [16] E. Todorov, T. Erez, and Y. Tassa, "MuJoCo: A physics engine for model-based control," in *2012 IEEE/RSJ International Conference on Intelligent Robots and Systems*. IEEE, 10 2012.
- [17] P. Schumacher, D. Häufle, D. Büchler, S. Schmitt, and G. Martius, "DEP-RL: Embodied exploration for reinforcement learning in over-actuated and musculoskeletal systems," in *The Eleventh International Conference on Learning Representations*, 2023.
- [18] J. Charaja, I. Wochner, P. Schumacher, W. Ilg, M. Giese, C. Maufroy, A. Bulling, S. Schmitt, and D. F. Haeufle, "Generating realistic arm movements in reinforcement learning: A quantitative comparison of reward terms and task requirements," in *2024 IEEE RAS/EMBS International Conference for Biomedical Robotics and Biomechanics (BioRob)*. IEEE, 2024.
- [19] M. Sapounaki, P. Schumacher, W. Ilg, M. Giese, C. Maufroy, A. Bulling, S. Schmitt, D. F. Haeufle, and I. Wochner, "Quantifying human upper limb stiffness responses based on a computationally efficient neuromusculoskeletal arm model," in *2024 IEEE RAS/EMBS International Conference for Biomedical Robotics and Biomechanics (BioRob)*. IEEE, 2024.
- [20] A. C. Pigg, J. Thompson-Westra, K. Mente, C. W. Maurer, D. Haubenberger, M. Hallett, and S. K. Charles, "Distribution of tremor among the major degrees of freedom of the upper limb in subjects with essential tremor," *Clinical Neurophysiology*, vol. 131, no. 11, pp. 2700–2712, nov 2020.
- [21] N. H. Bhanpuri, A. M. Okamura, and . Bastian, Amy J., "Predicting and correcting ataxia using a model of cerebellar function," *Brain*, vol. 137, no. 7, pp. 1931–1944, 2014.
- [22] K. Stollenmaier, I. Rist, F. Izzi, and D. F. Haeufle, "Simulating the response of a neuro-musculoskeletal model to assistive forces: implications for the design of wearables compensating for motor control deficits," in *2020 8th IEEE RAS/EMBS International Conference for Biomedical Robotics and Biomechanics (BioRob 2020)*. Piscataway, NJ: IEEE, Oct. 2020, pp. 779–784.
- [23] W. C. Pinheiro, H. B. Ferraz, M. C. F. Castro, and L. L. Menegaldo, "An opensim-based closed-loop biomechanical wrist model for subject-specific pathological tremor simulation," *IEEE Transactions on Neural Systems and Rehabilitation Engineering*, vol. 32, pp. 1100–1108, 2024.
- [24] T. Novacek, C. Marty, and M. Jirina, "Project multileap: Fusing data from multiple leap motion sensors," in *2021 IEEE 7th International Conference on Virtual Reality (ICVR)*, 2021, pp. 19–25.
- [25] Z. Hu, S. Schmitt, D. Haeufle, and A. Bulling, "Gazemotion: Gaze-guided human motion forecasting," in *Proceedings of the 2024 IEEE/RSJ International Conference on Intelligent Robots and Systems*, 2024.